Bright Subcycle Extreme Ultraviolet Bursts from a Single Dense Relativistic Electron Sheet

W. J. Ma (马文君),[1,*] J. H. Bin (宾建辉),[1,2] H. Y. Wang (王鸿勇),[2,3] M. Yeung,[4,5] C. Kreuzer,[1] M. Streeter,[6] P. S. Foster,[7,4] S. Cousens,[4] D. Kiefer,[1] B. Dromey,[4] X. Q. Yan (颜学庆),[3] J. Meyer-ter-Vehn,[2] M. Zepf,[4,5] and J. Schreiber[1,2,†]

[1]*Fakultät für Physik, Ludwig-Maximilians-University, Am Coulombwall 1, D-85748 Garching, Germany*
[2]*Max-Planck-Institute of Quantum Optics, Hans-Kopfermann-Strasse 1, D-85748 Garching, Germany*
[3]*State Key Laboratory of Nuclear Physics and Technology & Center of Applied Physics and Technology, Peking University, Beijing 100871, China*
[4]*Department of Physics and Astronomy, Queen's University Belfast, Belfast BT7 1NN, United Kingdom*
[5]*Helmholtz Institute Jena, 07743 Jena, Germany*
[6]*Blackett Laboratory, Imperial College London, London SW7 2AZ, United Kingdom*
[7]*Central Laser Facility, STFC Rutherford Appleton Laboratory, Chilton, Didcot OX11 0QX, United Kingdom*

(Received 17 March 2014; published 3 December 2014)

Double-foil targets separated by a low density plasma and irradiated by a petawatt-class laser are shown to be a copious source of coherent broadband radiation. Simulations show that a dense sheet of relativistic electrons is formed during the interaction of the laser with the tenuous plasma between the two foils. The coherent motion of the electron sheet as it transits the second foil results in strong broadband emission in the extreme ultraviolet, consistent with our experimental observations.

DOI: 10.1103/PhysRevLett.113.235002 PACS numbers: 52.38.-r

Controlling the motion of relativistic electrons is a powerful and flexible approach to producing bright, intense photon sources extending from the far infrared [1] to the x-ray domain [2]. Free electron lasers are currently the most brilliant extreme ultraviolet (XUV) and x-ray radiation facilities and routinely offer radiation bursts with durations of tens of femtoseconds, which can be further reduced to the femtosecond regime by tailoring the bunches [3,4]. Beyond classical accelerators, ultraintense laser interactions are of particular interest, as they allow one both to realize extremely compact electron accelerators [5,6] and to control the motion of the relativistic electrons coherently to produce bright sources of radiation, fully synchronized to an optical laser field [7,8].

Laser-driven sources are also particularly well suited to enter the attosecond regime [9,10]. In analogy to the microbunching that underlies the process in free electron lasers, ultraintense laser interactions with a foil target result in dense nanometer-scale electron bunches [11]. In general, a multicycle laser will produce a train of such extremely dense electron bunches, and their periodic relativistic motion results in a train of bright attosecond XUV and x-ray bursts [12,13].

Recent theoretical work by Wu and Meyer-ter-Vehn has gone beyond such periodic bunch structures and predicted that isolated relativistic electron sheets (RESs) can be produced [11,14,15] and exploited for the production of a new class of radiation—unipolar XUV pulses [16]. In these simulations, the formation of the RESs is achieved by the interaction of an ideal two-cycle Gaussian laser pulse with a peak intensity of $I_0 = 10^{21}$ W/cm^2 with a monolayer foil. Under such conditions, the strong ponderomotive force separates all electrons from the global Coulomb field of the remaining ions. All electrons then comove along the laser axis and form a RES with the electrons undergoing synchronous oscillations in the laser field. When approaching a second, thicker foil, placed in the beam path, the electrons are transmitted and the laser is reflected (or "shaken off"). Interestingly, if the laser is obliquely incident under an angle θ and *s*-polarized, all electrons gain momentum, *perpendicular* to the direction of polarization. This can be understood as the action of the $\boldsymbol{v} \times \boldsymbol{B}$ force of the obliquely reflected laser. A derivation is presented in Supplemental Material [17–25]. This rapid (over a quarter of the laser period) and unidirectional momentum gain gives rise to the emission of a burst of coherent radiation in form of an isolated half-cycle pulse in the XUV.

While the idealized interaction conditions considered by Wu and Meyer-ter-Vehn are still somewhat beyond current laser and target technology, we show that an isolated RES can be achieved with existing lasers and observe the emission of a bright, broadband continuum consistent with the production of a unipolar radiation pulse.

In our case, the two foils are separated by a tenuous plasma [Figs. 1(a) and 1(b)], and the first target is significantly thicker (initially 5 nm). In contrast to the theoretical paper, it does not serve to provide the RES by reaching the ponderomotive "blowout" condition [11]. Instead, the first foil acts as a "shutter" to shape the rising edge of the laser pulse by exploiting relativistic transparency [26]. Our simulations predict that an intense 50 fs pulse is transmitted with an extremely steep front rising to

peak intensity over about a single cycle. The RES is formed by the subsequent interaction of the steepened pulse with the tenuous plasma formed between the two foils by laser desorption [23] of contaminants on the second foil. Even though we have not directly characterized this tenuous plasma, we explain, in Supplemental Material [17], that such plasma is created due to the nanosecond pedestal of the laser. The strong ponderomotive force associated with the steep rising edge then sweeps up the electrons of this tenuous plasma similar to a snow plough [27,28] such that a dense RES is formed, copropagating with the laser front. In fact, we find that RES formation does not critically depend on plasma density and its shape.

From there on, the process is analogous to the original proposal. The second foil, 20 nm thick and $450n_c$ dense in the experiments, acts as a reflector for the copropagating laser and is sufficiently thin to allow the RES to be transmitted while thick enough to withstand the remaining prepulses and reflect the steepened main pulse.

Before we discuss the experimental observations, we consider simulations of the multistep interaction of the laser with a double-foil target and the expected radiative signal.

The two-dimensional (2D) particle-in-cell (PIC) simulations were carried out with the KLAP code [29] and correspond closely to our experimental conditions. The simulation box has a size of $80\lambda_L \times 40\lambda_L$ in the y-z plane with a resolution of 100 cells per laser wavelength λ_L. The two oblique foils are located at $z = 5\lambda_L$ and $z = 37\lambda_L$ on the central line at $y = 0$. Both are tilted by $\theta = 30°$. The first foil is assumed to have an exponential density profile peaked at $50n_c$ and a scale length of 50 nm (corresponding to a 5 nm solid foil with some preexpansion due to the laser prepulse). The second foil is modeled by a $200n_c$ steplike plasma with 50 nm thickness. The gap between the two foils is filled with dilute plasma at an electron density of $0.1n_c$. For the dilute plasma and the second foil, 200 and 40 macroparticles per cell were used, respectively. The laser pulse, polarized in x and propagating in the z direction, has a peak intensity of 2.1×10^{20} W/cm^2 with a Gaussian shape in space and time. Its full-width-at-half-maximum (FWHM) duration is 50 fs. The focal spot of 4 μm FWHM diameter was placed at the second foil.

Figure 1(c) shows the pulse after passing through the shutter foil at $T = 50T_L$. As mentioned above, the transmitted pulse amplitude rises to its maximum in approximately one optical cycle due to the sudden onset of relativistic transparency. The RES with near-critical density can be seen ahead of the laser front.

The momentum distribution of the electrons constituting the RES is shown in Fig. 1(e). The electrons have a broad momentum distribution up to $|p_{x0}|/(m_e c) \approx 10 \approx a_0$ and $|p_{z0}|/(m_e c) \approx 14$, where a_0 denotes the normalized vector potential of the laser field. Figure 1(f) shows the phase space at a later time, when the RES has completed its transit through the reflector foil. Notice that p_x has dropped to zero due to the vanishing laser field behind the second foil

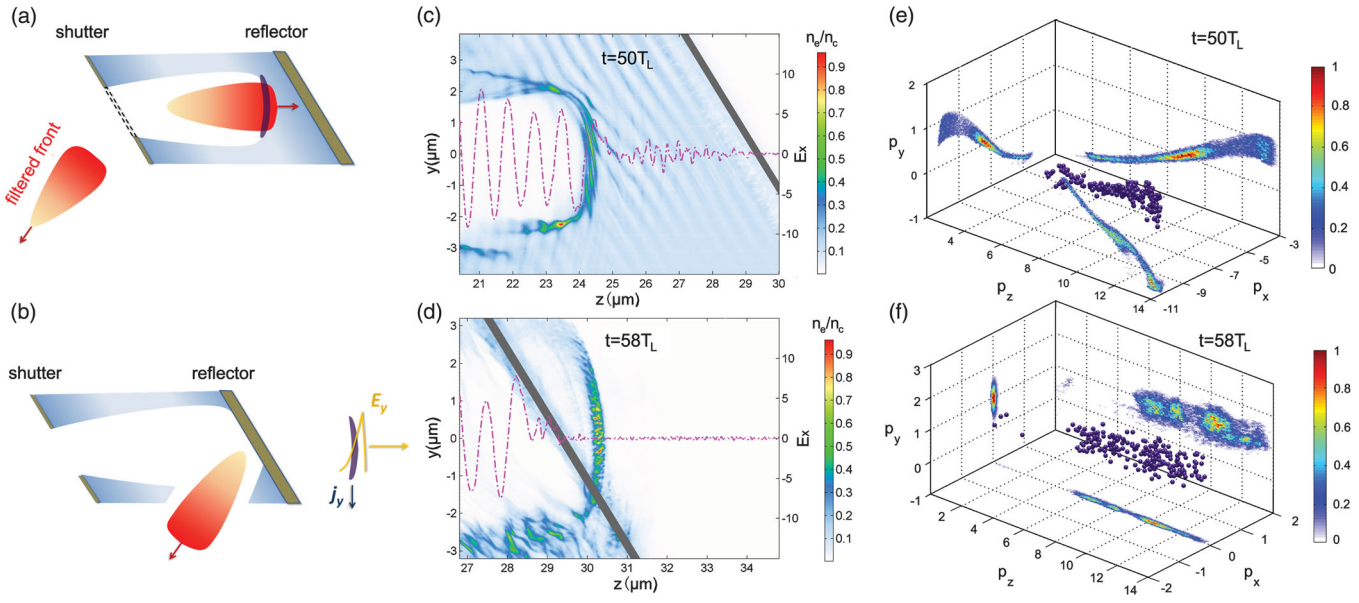

FIG. 1 (color). (a) The leading edge of the 50 fs laser pulse is reflected by the 5 nm thin foil. Relativistic transparency is induced at a certain intensity threshold, and the steepened pulse propagates through the low density plasma piling up electrons in a RES. (b) The second foil reflects the laser. The transmitted RES gains transverse momentum leading to half-cycle XUV emission. (c),(d) Snapshots of the electron density and laser field in the y, z plane during RES formation ($t = 50T_L$) and after shakeoff ($t = 58T_L$). (e),(f) Momentum phase space (p_x, p_y, p_z in units of $m_e c$) of RES electrons corresponding to frames (c) and (d). During shakeoff of the laser field, electrons lose their quiver momenta ($p_x = 0$) but pick up uniform momentum in the y direction ($p_y = 1.1 m_e c$). The RES with a diameter of $\sim$4 μm and maximum density $n_e \sim 10^{21}$/cc ($0.9n_c$) contains a charge of about 400 pC.

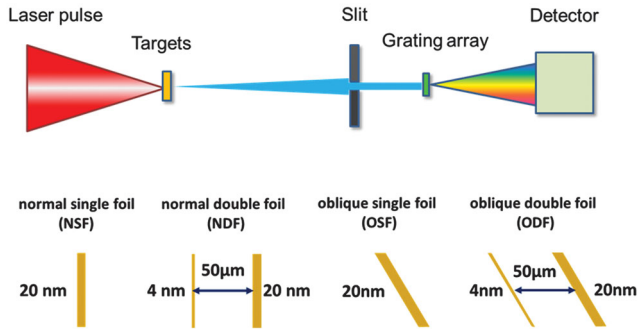

FIG. 2 (color). Experimental setup. The s-polarized laser pulse is focused on the four target configurations. XUV emission is spectrally resolved by gratings located behind a slit.

and that all RES electrons have picked up $p_y \approx m_e c$. The switch of momenta happens when the first dominant laser cycle is reflected and sweeps over the RES, i.e., over one-quarter of a laser wavelength ≈200 nm. The electrons in the RES are deflected by $p_y/p_z \approx 100$ mrad and must emit synchrotron radiation with a broad spectrum and critical frequency of ≈150 eV, corresponding to a spike of E_y in the time domain. Such a high-frequency field propagating with the RES is indeed observed in our simulation, even though the numerical resolution we could afford in the 2D simulation was insufficient to resolve its attosecond scale.

The experiment was performed at the Gemini facility, providing 50 fs laser pulses at 800 nm wavelength. A double plasma mirror system was used to enhance the contrast ratio to $>10^{10}$ at −10 ps. The on-target energy was about 5 J in a 4 μm FWHM spot with a peak intensity of 2×10^{20} W/cm^2. We assembled diamondlike carbon (DLC) foils either as single-foil (20 nm thick) or double-foil (4/20 nm) targets separated by 50 μm, in which case the focal spot was positioned onto the second foil (Fig. 2). DLC is stable up to 1100 °C in vacuum and can therefore withstand the irradiation by the 2–3 ns long amplified spontaneous emission at a level of 10^8 W/cm^2. The foil in focus is heated to several hundred degrees Celsius, resulting in fast desorption of contaminant atoms which form a gas plume (see Supplemental Material [17]). In case of the double foils, the gas is trapped within the sealed space between the two foils and ionized only when the steepened pulse arrives.

Several different configurations were tested experimentally: at normal incidence single and double foils (referred to as NSF and NDF, respectively) and at oblique incidence ($\theta = 30°$, the maximum angle allowed in our setup) single and double foils (OSF and ODF, respectively).

The XUV radiation was detected with an microchannel plate detector coupled to an angularly resolved spectrometer equipped with one 10 000 lines/mm SiN transmission grating to cover the spectral range of 3–30 nm and one 1000 lines/mm gold transmission grating for the range of 20–180 nm. The gold grating was positioned slightly off

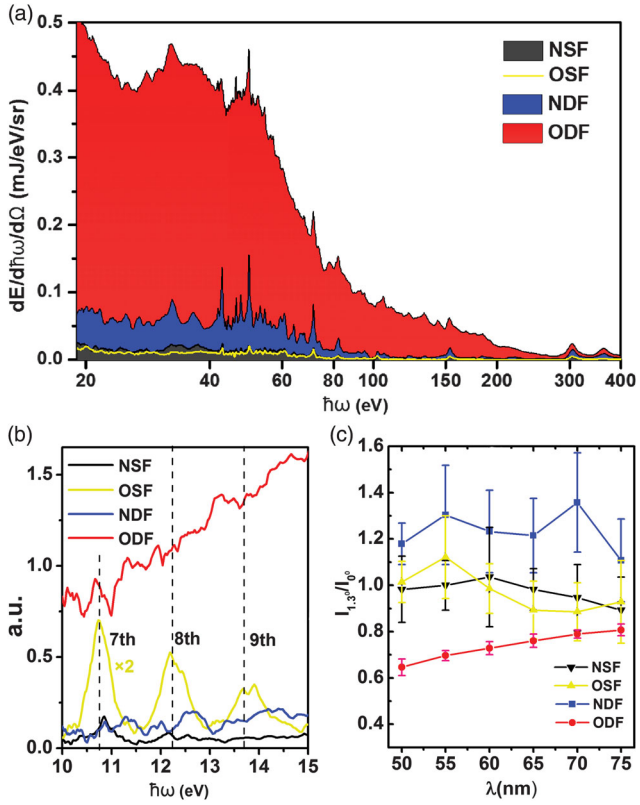

FIG. 3 (color). Experimental spectra in the range of (a) 18–400 and (b) 10–15 eV. Dashed lines mark the 7th, 8th, and 9th harmonics. Note that the spectra of (b) are recorded behind a 60 nm Al filter without calibration; they give only relative amplitudes for different target geometry, but not the actual shape of the spectra. (c) Ratio of off-axis to on-axis intensity, normalized to the case of OSF at 50 nm.

axis and allowed for an angular coverage of 1.3° around the laser axis.

Figures 3(a) and 3(b) show that over the observable spectral range from 10 to 400 eV the recorded spectra indeed strongly depend on target assembly and irradiation geometry. Regardless of the angle of incidence, single-foil targets produce weak emission extending up to 70 eV. The spectral modulations at multiples of the laser frequency between 10 and 15 eV indicate the well-known emission of XUV-pulse trains due to the repetitive and periodic generation of electron bunches [30]. When double-foil targets are irradiated at normal incidence, a slight increase in signal is observed. However, when the double-foil targets are tilted by an angle of 30° (laser is s polarized), a bright XUV continuum extending up to 280 eV is observed. Its spectral intensity is one order of magnitude larger over the complete spectral range accessible with the spectrometer, and the absence of modulation indicates the presence of only one dominant radiation burst. Note that the strength of the line emission resulting from recombination within the carbon plasma remains similar for all cases. The spectral intensity in Fig. 3(a) was calibrated by using the known energy of

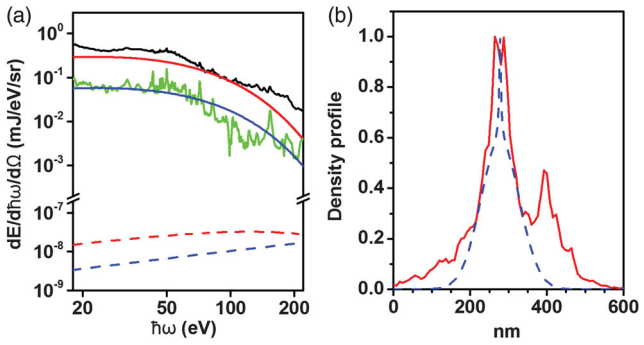

FIG. 4 (color). (a) Measured spectrum for ODF (black solid line) and NDF (green solid line). For comparison, spectra of coherent synchrotron emission in the yz (red solid line) and xz plane (blue solid line) are calculated by using values $\Delta p_y = 1.1 m_e c, \Delta p_x = 8 m_e c$ from the simulation at $T = 56 T_L$ and $p_z = 15 m_e c$, the blue dashed longitudinal density profile in (b), and a charge of 900 pC. The red dashed and blue dashed lines in (a) would result from completely incoherent emission. (b) Electron density profile used to calculate the spectra in (a) (blue dashed line), and the result of the PIC simulation at $T = 58 T_L$ (red solid line).

the carbon Ly-α line radiation (376 eV, $\approx 10^{-4}$ of the laser energy [21]) which is isotropically emitted from a 20 nm NSF target (see Supplemental Material [17]).

Meanwhile, the large intensity indicates a high degree of coherence of the emission process. As shown in Fig. 4, the spectral intensity of incoherent synchrotron radiation emitted by an RES with a charge of 400 pC (the value observed in our simulation in Fig. 1) would be 6–7 orders of magnitude lower than the experimentally observed spectral intensity, demonstrating that the process that gives rise to this continuum must be a coherent process. The corresponding spectral shape is then given by the form factor, i.e., the longitudinal Fourier transform of the emitting electron sheet (see Supplemental Material [17]). One possible electron density distribution that reproduces the measured spectrum is shown in Fig. 4(b). It is remarkably similar to the electron density profile obtained from the simulation. The absolute magnitude of the spectral intensity would suggest as much as 900 pC of charge, again close to the value obtained from the simulations.

Information on the transverse coherence of the emission process can be obtained from the angular divergence of the radiation measured in the wavelength range 50–75 nm. Only the radiation from obliquely irradiated double-foil targets shows clear evidence of directed emission, indicating spatial (transverse) coherence. The emission cone angle can be estimated from our data by taking the ratio of the 1.3°-off-axis to the on-axis intensity $I_{1.3°}/I_{0°}$. For a fixed source size, one would expect the beam divergence to depend on the wavelength, and indeed the ratio $I_{1.3°}/I_{0°}$ rises from 0.65 to 0.78 as the wavelength increases from 50 to 75 nm. More quantitatively, the curve can be reproduced by an Airy far-field pattern with a FWHM divergence of 3.2°, suggesting that the emitted radiation has a flat phase over a source with a diameter of $D = 0.9$ μm. This diameter determines the distance $L_d \sim D^2/(c\tau)$ over which any half-cycle pulse maintains its half-cycle nature before evolving into a single-cycle pulse due to diffraction-induced transformation. In the limit of a zero-thickness RES, theory [16] predicts that the width of the pulse in our case is $\tau = m_e c/(\gamma_z e E_s) \approx 40$ as, where $E_s = n_e e d/\varepsilon_0$ is the electrostatic field created by the RES areal charge density $n_e e d$. By using these values, $L_d \approx 670$ μm is obtained. In reality, this distance will be shorter, but the pulse could be recovered to some extent by appropriate refocusing [31]. Assuming that the continuum from 30 to 280 eV observed from the ODF is emitted in a cone with a 56 mrad FWHM angle, we estimate a pulse energy of 15 μJ or 3×10^{-5} of the initial laser energy.

In conclusion, we have demonstrated that coherent radiation bursts consistent with the radiation of a single relativistic electron sheet can be produced by using double-foil targets at oblique incidence. This broadband source of continuum radiation is emitted as a half-cycle pulse and represents a new class of ultrafast radiation source with applications in atomic physics [32], solid state physics [33], and high-energy-density matter physics [34].

This work was supported by the DFG-funded Cluster of Excellence MAP, EPSRC, and National Basic Research Program of China (2013CBA01502). The authors acknowledge the excellent support of the Gemini and CLF staff, the help of Dr. Matthias Kling for providing the silicon transmission grating, and the work of the target fabrication lab of LMU.

*Wenjun.Ma@physik.uni-muenchen.de
†Joerg.Schreiber@lmu.de

[1] P. Michel *et al.*, The Rossendorf IR-FEL ELBE, http://inspirehep.net/record/737745?ln=en.
[2] E. Hand, Nature (London) **461**, 708 (2009).
[3] I. Grguras *et al.*, Nat. Photonics **6**, 852 (2012).
[4] Y. Ding *et al.*, Phys. Rev. Lett. **109**, 254802 (2012).
[5] W. P. Leemans, B. Nagler, A. J. Gonsalves, C. Toth, K. Nakamura, C. G. R. Geddes, E. Esarey, C. B. Schroeder, and S. M. Hooker, Nat. Phys. **2**, 696 (2006).
[6] A. Pukhov, Z. M. Sheng, and J. Meyer-ter-Vehn, Phys. Plasmas **6**, 2847 (1999).
[7] S. V. Bulanov, T. Z. Esirkepov, M. Kando, A. S. Pirozhkov, and N. N. Rosanov, Phys. Usp. **56**, 429 (2013).
[8] F. Quere *et al.*, Nat. Phys. **3**, 424 (2007).
[9] F. Krausz and M. Ivanov, Rev. Mod. Phys. **81**, 163 (2009).
[10] U. Teubner and P. Gibbon, Rev. Mod. Phys. **81**, 445 (2009).
[11] V. V. Kulagin, V. A. Cherepenin, M. S. Hur, and H. Suk, Phys. Rev. Lett. **99**, 124801 (2007).
[12] B. Dromey *et al.*, Nat. Phys. **8**, 804 (2012).
[13] D. Kiefer *et al.*, Nat. Commun. **4**, 1763 (2013).

[14] V. V. Kulagin, V. A. Cherepenin, Y. V. Gulyaev, V. N. Kornienko, K. H. Pae, V. V. Valuev, J. Lee, and H. Suk, Phys. Rev. E **80**, 016404 (2009).
[15] H. C. Wu, J. Meyer-ter-Vehn, J. Fernandez, and B. M. Hegelich, Phys. Rev. Lett. **104**, 234801 (2010).
[16] H. C. Wu and J. Meyer-ter-Vehn, Nat. Photonics **6**, 304 (2012).
[17] See Supplemental Material at http://link.aps.org/supplemental/10.1103/PhysRevLett.113.235002, for derivation of the birth of the transverse momentum, the calibration of the spectrometer, the origin of the tenuous plasma, and the coherent synchrotron emission calculation, which includes Refs. [18–25].
[18] H. C. Wu and J. Meyer-ter-Vehn, Eur. Phys. J. D **55**, 443 (2009).
[19] H. W. Schnopper, L. P. Vanspeybroeck, J. P. Delvaille, A. Epstein, E. Kallne, R. Z. Bachrach, J. Dijkstra, and L. Lantward, Appl. Opt. **16**, 1088 (1977).
[20] S. G. Tomlin, J. Phys. D: Appl. Phys. **1**, 1667 (1968).
[21] A. A. Andreev, U. Teubner, I. V. Kurnin, and E. Forster, Appl. Phys. B **70**, 505 (2000).
[22] T. Tajima, D. Habs, and X. Yan, Rev. Accel. Sci. Techol. **02**, 201 (2009).
[23] M. Handschuh, S. Nettesheim, and R. Zenobi, J. Phys. Chem. B **103**, 1719 (1999).
[24] J. Robertson, Mater. Sci. Eng. R **37**, 129 (2002).
[25] J. D. Jackson, *Classical Electrodynamics* (Wiley, New York, 1999).
[26] S. Palaniyappan *et al.*, Nat. Phys. **8**, 763 (2012).
[27] Q. Kong, S. Miyazaki, S. Kawata, K. Miyauchi, K. Nakajima, S. Masuda, N. Miyanaga, and Y. K. Ho, Phys. Plasmas **10**, 4605 (2003).
[28] C. S. Liu and V. K. Tripathi, Phys. Plasmas **12**, 043103 (2005).
[29] H. Y. Wang, C. Lin, Z. M. Sheng, B. Liu, S. Zhao, Z. Y. Guo, Y. R. Lu, X. T. He, J. E. Chen, and X. Q. Yan, Phys. Rev. Lett. **107**, 265002 (2011).
[30] M. Yeung *et al.*, Phys. Rev. Lett. **112**, 123902 (2014).
[31] A. E. Kaplan, J. Opt. Soc. Am. B **15**, 951 (1998).
[32] E. Goulielmakis *et al.*, Nature (London) **466**, 739 (2010).
[33] A. L. Cavalieri *et al.*, Nature (London) **449**, 1029 (2007).
[34] S. M. Vinko *et al.*, Nature (London) **482**, 59 (2012).